

## **Improving electron mobility in MoS<sub>2</sub> field-effect transistors by optimizing the interface contact and enhancing the channel conductance through local structural phase transition**

Zhaofang Cheng<sup>1,2</sup>, Shaodan He<sup>1</sup>, Xiaona Han<sup>1</sup>, Xudong Zhang<sup>1</sup>, Lina Chen<sup>1</sup>, Shijun Duan<sup>1</sup>, Shimin Zhang<sup>1</sup>, and Minggang Xia<sup>1,2,3,\*</sup>

<sup>1</sup> *Department of Applied Physics, School of Physics, Xi'an Jiaotong University, Shaanxi 710049, People's Republic of China.*

<sup>2</sup> *MOE Key Laboratory for Nonequilibrium Synthesis and Modulation of Condensed Matter, School of Physics, Xi'an Jiaotong University, 710049, People's Republic of China.*

<sup>3</sup> *Laboratory of Nanostructure and Physics Properties, Key Laboratory for Quantum Information and Optoelectronic Quantum Devices of Shaanxi Province, School of Physics, Xi'an Jiaotong University, 710049, People's Republic of China.*

(Some figures in this article are in color only in the electronic version.)

This research did not receive any specific grant from funding agencies in the public, commercial, or not-for-profit sectors.

\* Address correspondence to: [xiamg@mail.xjtu.edu.cn](mailto:xiamg@mail.xjtu.edu.cn)

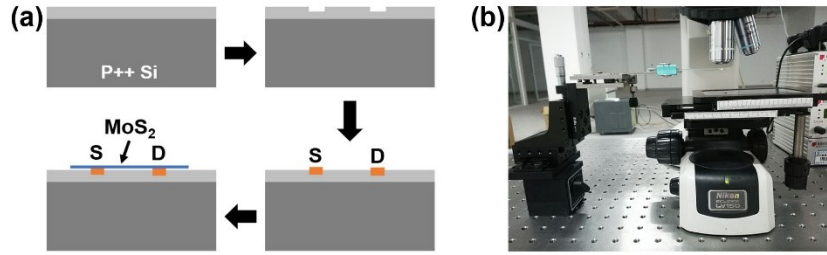


Fig. S1. (a) The fabrication process of MoS<sub>2</sub> vdW FETs. 285 nm silicon oxide (SiO<sub>2</sub>) substrate cleaned with acetone and isopropyl alcohol (IPA), the bottom is p-type heavily doped Si (p+ Si), which can be used as a back gate; two sites were etched on SiO<sub>2</sub> and 80 nm thick Au electrodes were deposited as source and drain electrodes, here there was a small gap of about 5 nm between the sample and the electrode, which facilitated the subsequent entry of oxygen plasma; About 2-3 layers of MoS<sub>2</sub> channel are transferred onto the electrodes, where an optical microscope is used to align the MoS<sub>2</sub> sample and electrodes for anchored transfer (b).

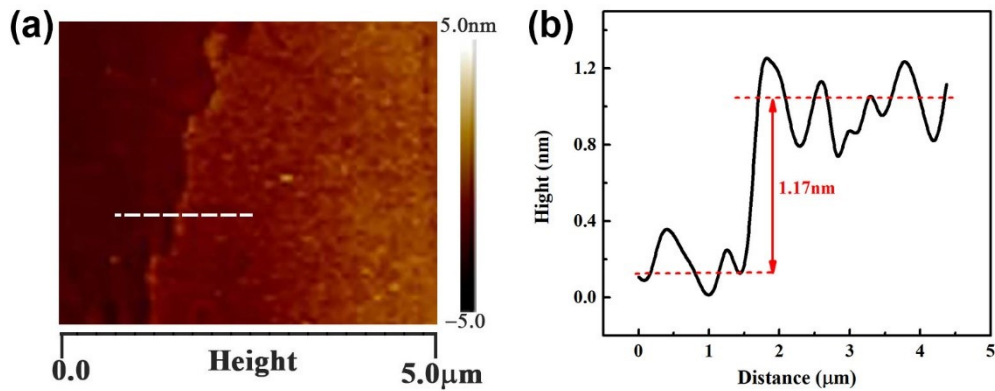


Fig. S2. (a) AFM spectra of MoS<sub>2</sub> channel in MoS<sub>2</sub> vdW device. (b) A height profile is extracted along the white line shown in panel (a). The MoS<sub>2</sub> domain thickness is 1.17 nm, equal to 2 monolayer thickness.

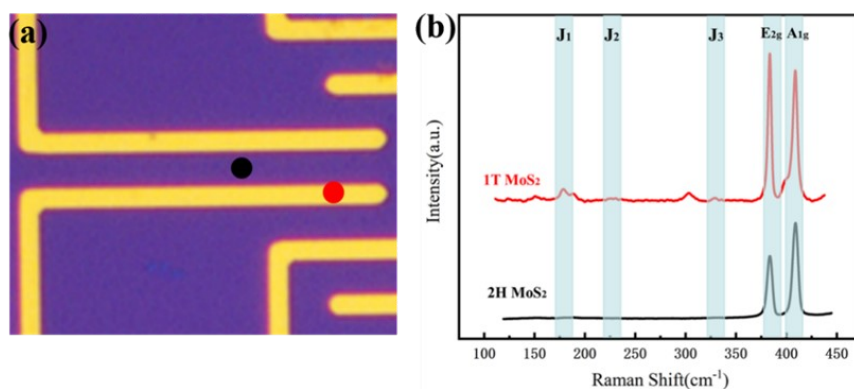


Fig. S3. Raman spectra (b) acquired from different regions highlighted in optical image of MoS<sub>2</sub> vdW devices (a) after O<sub>2</sub> plasma treatment for 1 s. The 1T phase transition of MoS<sub>2</sub> occurs in the region in contact with the Au electrodes firstly, which may be attributable to the catalytic effect of Au. Here Au provides free electrons in the plasma process, which can accelerate the kinetic process of the oxidation reaction, thus reducing the reaction energy barrier of oxygen doping.

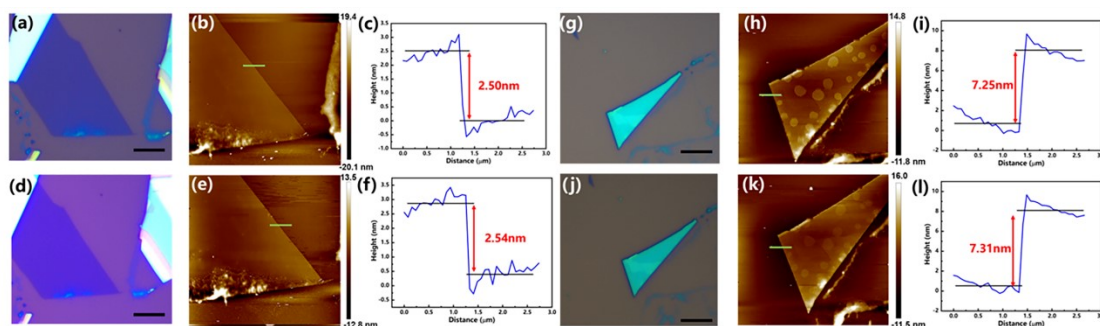


Fig. S4. The impact of O<sub>2</sub> plasma on the surface morphology of MoS<sub>2</sub>. The optical images of few-layer MoS<sub>2</sub> nanosheets before (a, g) and after (d, j) being treated by oxygen plasma for 3 s. Scale bar: 10 μm. There is minimal change in color of the MoS<sub>2</sub>, suggesting that the sample's surface did not experience significant thinning due to the plasma etching. The AFM characterizations of MoS<sub>2</sub> nanosheets before (b, h) and after (e, k) being treated by oxygen plasma for 3 s. The samples exhibit flat surfaces and similar thicknesses before (c, i) and after (f, l) oxygen plasma treatment, indicating that our soft oxygen plasma mainly plays a role of doping on MoS<sub>2</sub> samples, with almost no etching effect.

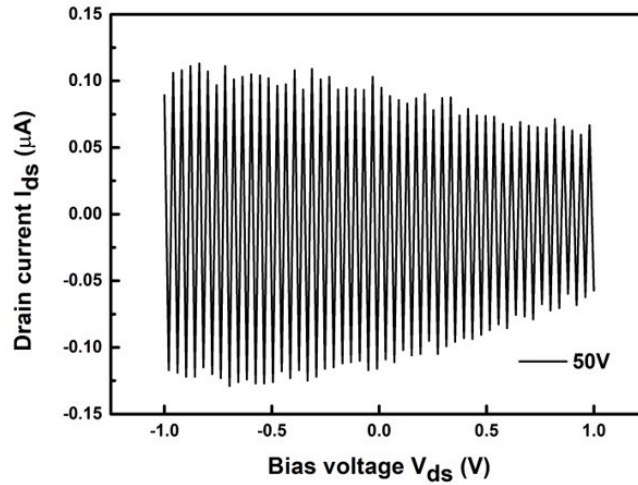


Fig. S5. Measurement of the leakage currents through the S or D electrodes and back gate.

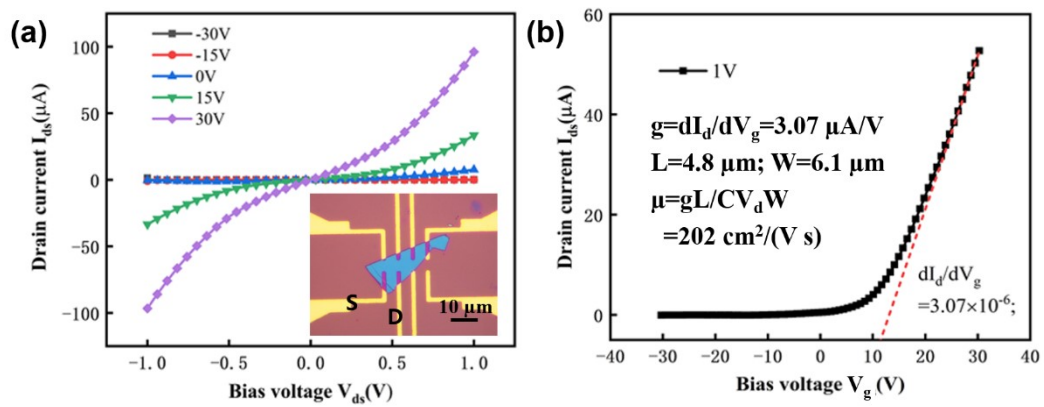


Fig. S6. Electronic characteristic curves of MoS<sub>2</sub> FET device2 after oxygen plasma exposure with 10 s. (a)  $I_{ds}$ - $V_{ds}$  characteristics up to  $V_{ds}=1$  V and  $V_g$  ranging from  $-30$  V to  $30$  V. Inset: Optical image of the MoS<sub>2</sub> device with corresponding working principle. (b) Corresponding  $I_{ds}$ - $V_g$  characteristics, exhibiting high electron mobility.

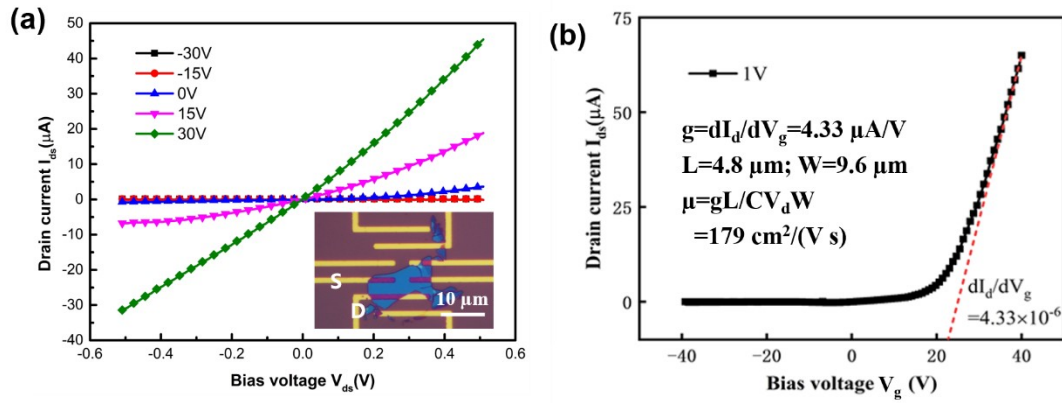


Fig. S7. Electrical characteristic curves of MoS<sub>2</sub> FET device3 after 5 s oxygen plasma exposure. (a)  $I_{ds}$ - $V_{ds}$  characteristics up to  $V_{ds}=0.5$  V and  $V_g$  ranging from  $-30$  V to  $30$  V. Inset: Optical image of the MoS<sub>2</sub> device3 with corresponding working principle. (b) Corresponding  $I_{ds}$ - $V_g$  characteristic curves.

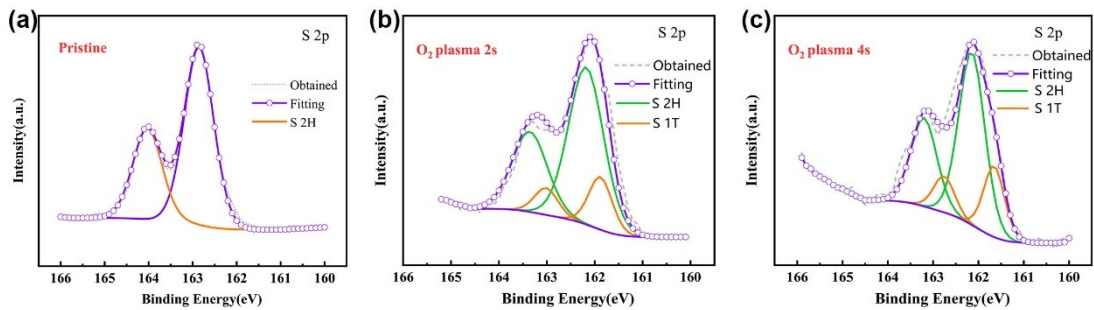


Fig. S8. XPS spectra showing S 2p core level peak regions for the pristine (a) and plasma-treated MoS<sub>2</sub> (b-d). The fitting green and orange curves represent the contributions of 2H and 1T phases to the S 2p peaks. For the pristine MoS<sub>2</sub>, the convoluted spectra of S 2p show two prominent peaks at 162.7 and 164.0 eV, respectively. After oxygen plasma exposure of MoS<sub>2</sub> from 2 s to 4 s, the peak intensity of 1T-S 2p peaks gradually enhance, which indicates the increase of 1T domain concentration in MoS<sub>2</sub>.

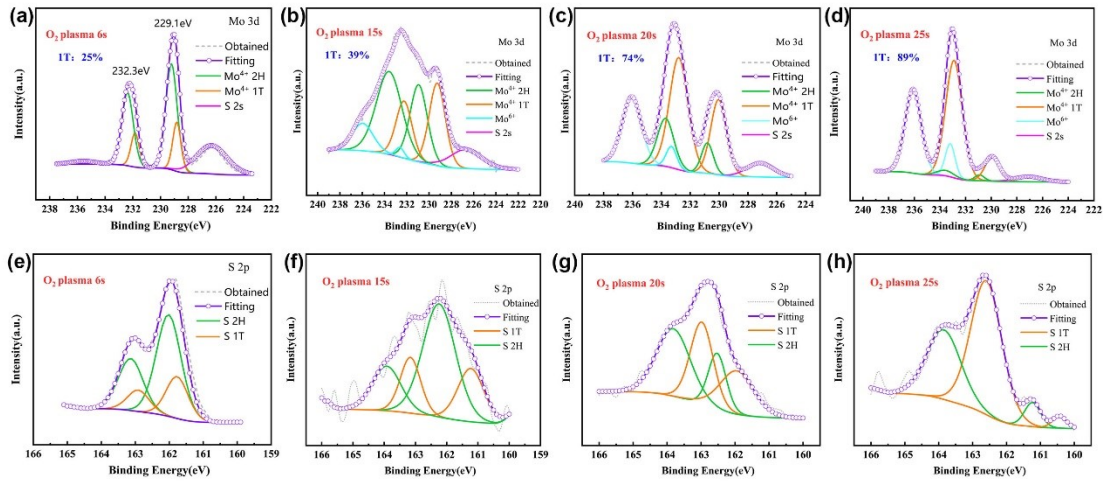


Fig. S9. XPS characterizations of Mo 3d (a-d) and S 2p (e-h) core level peak regions for the MoS<sub>2</sub> after O<sub>2</sub> plasma treatment with time varying from 6-25 s. We observed that the 1T phase concentrations continue to increase from 25% to 89% as the plasma treatment time increased.

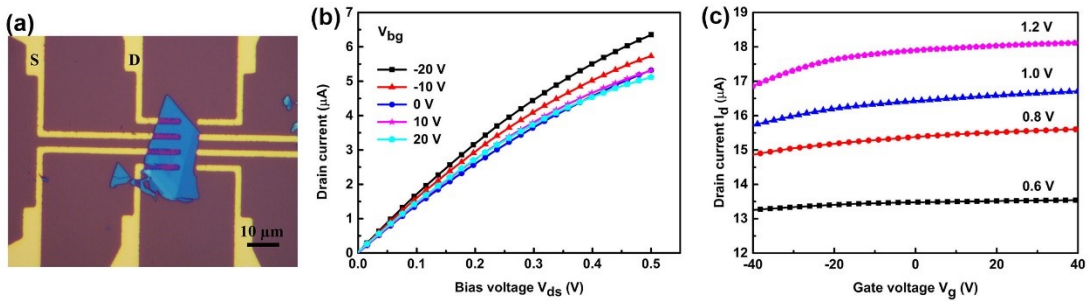


Fig. S10. I-V characteristic curve of MoS<sub>2</sub> device4 with plasma treatment time exceeding 6 s. (a) Optical image of MoS<sub>2</sub> device4. Here, the channel length (L) and width (W) are 2.8 μm and 6.5 μm, respectively. (b-c) Output (b) and transfer (c) characteristics of MoS<sub>2</sub> device4 with plasma treatment time exceeding 6 s.

**Table S1 Literature survey of electrical performance of MoS<sub>2</sub> devices**

Device	method	Contact Resistance (k $\Omega$ $\mu$ m)	Conductivity (S m <sup>-1</sup> )	Mobility (cm <sup>2</sup> V <sup>-1</sup> s <sup>-1</sup> )	On/off ratio	Ref
MoS <sub>2</sub> FET	vdW contacts, Pt	430	4.2	44	10 <sup>7</sup>	[1]
MoS <sub>2</sub> FET	vdW contacts, Ag	2.3	~140	-	10 <sup>7</sup>	[2]
MoS <sub>2</sub> FET	vdW contacts, In	3 $\pm$ 0.3(monolayer) 0.8 $\pm$ 0.2(few layers)	20	167 $\pm$ 20	-	[3]
MoS <sub>2</sub> FET	1T contacts	0.2-0.3	85	50	>10 <sup>7</sup>	[4]
MoS <sub>2</sub> FET	1T contacts	0.2	~20	56	-	[5]
MoS <sub>2</sub> FET	Bi contacts	123	100-373	20	>10 <sup>7</sup>	[6]
MoS <sub>2</sub> FET	vdW contacts, Graphene	115	~5	35	>10 <sup>8</sup>	[7]
MoS <sub>2</sub> FET	Au contacts	6.5	~140	20	-	[8]
MoS <sub>2</sub> FET	Re doping	26.65	0.7	-	-	[9]
MoS <sub>2</sub> FET	vdW contacts, Graphene	2-20	~1	40-120	-	[10]
MoS <sub>2</sub> FET	vdW contacts BN/Au	1.8	~30 (V <sub>G</sub> =40V)	73	-	[11]
MoS <sub>2</sub> FET	Au /Al <sub>2</sub> O <sub>3</sub> / TiO <sub>2</sub>	5.4	~5	-	-	[12]
MoS <sub>2</sub> F ET	Thiol- Molecules	25.2	~10 (V <sub>G</sub> =40 V)	-	-	[13]
MoS <sub>2</sub> FET	Cl-doped	0.5	~160 (V <sub>G</sub> =4 5V)	60	4*10 <sup>6</sup>	[14]
MoS <sub>2</sub> FET	Mo/Au	2	~35 (V <sub>G</sub> =30 V)	27	-	[15]
MoS <sub>2</sub> FET	vdW 1T contacts	4	83.8	237	10 <sup>4</sup>	This work

**Table S2 Comparison of MoS<sub>2</sub> FETs before and after plasma treatment**

MoS <sub>2</sub> FETs	Property	Contact Resistances (k $\Omega$ )	Transconductance ( $\mu$ A/V)	Mobility (cm <sup>2</sup> /V s)	On/off ratio
Device1 (L=3 $\mu$ m)	Before plasma treatment	477.2	0.1	7	$\sim 10^2$
	O <sub>2</sub> plasma 3s	4.0	4.3	237	$\sim 10^4$
Device2 (L=4.8 $\mu$ m)	O <sub>2</sub> plasma 10s	--	3.1	202	$\sim 10^3$
Device3 (L=4.8 $\mu$ m)	O <sub>2</sub> plasma 5s	--	4.3	179	$\sim 10^3$
Device4 (L=2.8 $\mu$ m)	Before plasma treatment	--	0.2	7	$\sim 10^2$
	O <sub>2</sub> plasma 2s	--	0.9	55	$\sim 10^3$
	O <sub>2</sub> plasma 4s	--	2.6	185	$\sim 10^4$

**References**

- [1] Y. Wang, J.C. Kim, Y. Li, K.Y. Ma, S. Hong, M. Kim, H. S. Shin, H.Y. Jeong, M. Chhowalla, P-type electrical contacts for 2D transition-metal dichalcogenides, *Nature* 610 (2022) 61-66.
- [2] X. Yang, J.Li, R. Song, B. Zhao, J. Tang, L. Kong, H. Huang, Z. Zhang, L. Liao, Y. Liu, X. Duan., X. Duan, Highly reproducible van der Waals integration of two-dimensional electronics on the wafer scale, *Nat. Nanotechnol.* 18 (2023) 471.
- [3] Y. Wang, J.C. Kim, R.J. Wu, J. Martinez, X. Song, J. Yang, F. Zhao, K.A. Mkhoyan, H.Y. Jeong, M. Chhowalla, Van der Waals contacts between three-dimensional metals and two-dimensional semiconductors, *Nature* 568 (2019) 70.
- [4] R. Kappera, D.Voiry, S.E.Yalcin, B. Branch, G. Gupta, A.D. Mohite, M. Chhowalla, Phase-engineered low-resistance contacts for ultrathin MoS<sub>2</sub> transistors, *Nat. Mater.* 13 (2014) 1128-1134.
- [5] R. Kappera, D. Voiry, S.E. Yalcin, W. Jen, M. Acerce, S. Torrel, B. Branch, S. Lei, W. Chen, S. Najmaei, J. Lou, P.M. Ajayan, G. Gupta, A.D. Mohite, M. Chhowalla, Metallic 1T phase source/drain electrodes for field effect transistors from chemical vapor deposited MoS<sub>2</sub>, *Apl Mater.* 2 (2014) 092516.
- [6] P.-C. Shen, C. Su, Y. Lin, A.-S. Chou, C.-C. Cheng, J.-H. Park, M.-H. Chiu, A.-Y. Lu, H.-L. Tang, M.M. Tavakoli, G. Pitner, X. Ji, Z. Cai, N. Mao, J. Wang, V. Tung, J. Li, J. Bokor, A. Zettl, C.-I. Wu, T. Palacios, L.-J. Li, J. Kong, Ultralow contact resistance between semimetal and monolayer semiconductors, *Nature* 593 (2021) 211.
- [7] S.-S. Chee, D. Seo, H. Kim, H. Jang, S. Lee, S.P. Moon, K.H. Lee, S.W. Kim, H. Choi, M.-H. Ham, Lowering the schottky barrier height by graphene/Ag electrodes for high-mobility MoS<sub>2</sub> field-effect transistors, *Adv. Mater.* 31 (2019) 1804422.
- [8] K.K.H. Smithe, C.D. English, S.V. Suryavanshi, E. Pop, Intrinsic electrical transport and performance projections of synthetic monolayer MoS<sub>2</sub> devices, *2D Mater.* 4(2017) 011009.
- [9] J. Gao, Y.D. Kim, L. Liang, J.C. Idrobo, P. Chow, J. Tan, B. Li, L. Li, B.G. Sumpter, T.-M. Lu, V. Meunier, J. Hone, N. Koratkar, Transition-metal substitution doping in synthetic atomically thin



semiconductors, *Adv. Mater.* 28 (2016) 9735.

[10] X. Cui, G.-H. Lee, Y.D. Kim, G. Arefe, P.Y. Huang, C.-H. Lee, D.A. Chenet, X. Zhang, L. Wang, F. Ye, F. Pizzocchero, B.S. Jessen, K. Watanabe, T. Taniguchi, D.A. Muller, T. Low, P. Kim, J. Hone, Multi-terminal transport measurements of MoS<sub>2</sub> using a van der Waals heterostructure device platform, *Nat. Nanotech.* 10 (2015) 534-540.

[11] J. Wang, Q. Yao, C.-W. Huang, X. Zou, L. Liao, S. Chen, Z. Fan, K. Zhang, W. Wu, X. Xiao, C. Jiang, W.-W. Wu, High mobility MoS<sub>2</sub> transistor with low schottky barrier contact by using atomic thick h-BN as a tunneling layer, *Adv. Mater.* 28 (2016) 8302-8308.

[12] W. Park, Y. Kim, S.K. Lee, U. Jung, J.H. Yang, C. Cho, Y.J. Kim, S.K. Lim, I.S. Hwang, H.-B.-R. Lee, B.H. Lee, Contact Resistance Reduction using Fermi Level De-pinning Layer for MoS<sub>2</sub> FETs, 2014 IEEE International Electron Devices Meeting, San Francisco, CA, USA (2014) 5.1.1-5.1.4.

[13] K. Cho, J. Pak, J.-K. Kim, K. Kang, T.-Y. Kim, J. Shin, B.Y. Choi, S. Chung, T. Lee, Contact-engineered electrical properties of MoS<sub>2</sub> field-effect transistors via electively deposited thiol-molecules, *Adv. Mater.* 30 (2018) 1705540.

[14] L. Yang, K. Majumdar, H. Liu, Y. Du, H. Wu, M. Hatzistergos, P.Y. Hung, R. Tieckelmann, W. Tsai, C. Hobbs, P.D. Ye, Chloride molecular doping technique on 2D materials: WS<sub>2</sub> and MoS<sub>2</sub>, *Nano Lett.* 14 (2014) 6275-6280.

[15] J. Kang, W. Liu, K. Banerjee, High-performance MoS<sub>2</sub> transistors with low-resistance molybdenum contacts, *Appl. Phys. Lett.* 104 (2014) 093106.